NAVAL AIR WARFARE CENTER AIRCRAFT DIVISION
PATUXENT RIVER, MARYLAND

TECHNICAL INFORMATION MEMORANDUM

REPORT NO: NAWCADPAX/TIM-2014/292

FERRIUM M54 STEEL

by

E. U. Lee
M. Stanley
B. Pregger
C. Lei
E. Lipnickas

18 March 2015

DEPARTMENT OF THE NAVY
NAVAL AIR WARFARE CENTER AIRCRAFT DIVISION
PATUXENT RIVER, MARYLAND

NAWCADPAX/TIM-2014/292
18 March 2015

FERRIUM M54 STEEL

by

E. U. Lee
M. Stanley
B. Pregger
C. Lei
E. Lipnickas

RELEASED BY:

Darrel R Tenney 18 Mar 2015

DARREL R. TENNEY, JR. / AIR-4.3.4/ DATE
Head, Materials Engineering Division
Naval Air Warfare Center Aircraft Division

REPORT DOCUMENTATION PAGE

Form Approved
OMB No. 0704-0188

1. REPORT DATE	2. REPORT TYPE	3. DATES COVERED
18 March 2015	Technical Information Memorandum	2014

4. TITLE AND SUBTITLE	5a. CONTRACT NUMBER
Ferrium M54 Steel	5b. GRANT NUMBER
	5c. PROGRAM ELEMENT NUMBER

6. AUTHOR(S)	5d. PROJECT NUMBER
E. U. Lee M. Stanley B. Pregger C. Lei E. Lipnickas	5e. TASK NUMBER
	5f. WORK UNIT NUMBER

7. PERFORMING ORGANIZATION NAME(S) AND ADDRESS(ES)	8. PERFORMING ORGANIZATION REPORT NUMBER
Naval Air Warfare Center Aircraft Division 22347 Cedar Point Road, Unit #6 Patuxent River, Maryland 20670-1161	NAWCADPAX/TIM-2014/292

9. SPONSORING/MONITORING AGENCY NAME(S) AND ADDRESS(ES)	10. SPONSOR/MONITOR'S ACRONYM(S)
Naval Air Systems Command 47123 Buse Road Unit IPT Patuxent River, Maryland 20670-1547	11. SPONSOR/MONITOR'S REPORT NUMBER(S)

12. DISTRIBUTION/AVAILABILITY STATEMENT

Approved for public release; distribution is unlimited.

13. SUPPLEMENTARY NOTES

14. ABSTRACT

Bare and Zn-14% Ni alloy coated Ferrium M54 steels were studied to clarify their mechanical, fatigue, and stress corrosion cracking (SCC) properties. Compared to the currently available high strength and high toughness steel, AerMet 100, this steel has much greater SCC resistance, but similar mechanical properties and susceptibility to corrosion fatigue. The Zn-14% Ni alloy coating appears to provide the steel some protection against hydrogen embrittlement/SCC and corrosion fatigue in aqueous 3.5% NaCl solution of pH 7.3. The fatigue crack growth mechanisms of the bare and coated steels are striation formation in air, and a combination of striation formation and intergranular cracking in aqueous 3.5% NaCl solution.

15. SUBJECT TERMS

Ferrium M54; Mechanical; Fatigue; Stress Corrosion Cracking (SCC)

16. SECURITY CLASSIFICATION OF:			17. LIMITATION OF ABSTRACT	18. NUMBER OF PAGES	19a. NAME OF RESPONSIBLE PERSON
a. REPORT	b. ABSTRACT	c. THIS PAGE			E. U .Lee
Unclassified	Unclassified	Unclassified	SAR	49	19b. TELEPHONE NUMBER (include area code) 301-342-8069

Standard Form 298 (Rev. 8-98)
Prescribed by ANSI Std. Z39-18

SUMMARY

Bare and Zn-14% Ni alloy coated specimens of Ferrium M54 steel were subjected to electrochemical measurement, microstructure examination, mechanical testing in air, fatigue testing in both air and aqueous 3.5% NaCl solution, SCC testing in an aqueous 3.5% NaCl solution, and SEM fractograph examination. The results indicate that, compared to AerMet 100 steel, this steel possesses similar high strength and high toughness, much higher SCC resistance in aqueous 3.5% NaCl solution, and similar fatigue strength in air and aqueous 3.5% NaCl solution. The Zn-14% Ni alloy coating was found to provide some protection of the substrate Ferrium M54 steel against SCC and corrosion fatigue in aqueous 3.5% NaCl solution.

Contents

Page No.

ACKNOWLEDGEMENTS

The support for this study from the NISE Research Program is gratefully acknowledged. Furthermore, the authors appreciate the NAE Chief Technology Officer, Dr. James B. Sheehy, and the Lead Air Vehicle Engineering Technologist, Mr. Jerry Rubinsky for their guidance and interest. The authors also thank Mr. Craig Matzdorf for insightful discussions on coating and Mr. Robert Taylor for his kind counsel on fatigue crack growth testing.

INTRODUCTION

High strength steels developed in the 1940's and 1950's, such as 4340* and 300M*, have been utilized for many structural components. However, steels such as these have high strength but low toughness have been found to be inadequate for highly stressed structural components. In the early 1990's, a Co-Ni alloy steel, AerMet 100*, was developed which had a good combination of high strength and high toughness, and has been employed for fracture critical components, such as aircraft landing gear. In 2002, a new steel, Ferrium M53, was developed. Compared to AerMet 100 steel, the SCC resistance is greater (K_{ISCC} = 35 ksi√in.), but the fracture toughness (K_{IC} = 70 ksi√in.) and the yield strength (228 ksi) are lower. In 2011, a modification of this steel improved the properties further to have the properties similar to or better than those of AerMet 100 at a lower cost. This most recent steel is called M54* and its properties remain to be fully characterized.

The aforementioned high strength steels have common undesirable characteristics. They are intrinsically susceptible to corrosion in aggressive environments and to delayed fracture attributed to hydrogen embrittlement and SCC. To prevent these types of degradation, many high strength steel components are protected with sacrificial electroplated coatings. However, the electroplating process itself can induce detrimental side effects, such as hydrogen embrittlement and/or SCC.

Hydrogen embrittlement is a process in which atomic hydrogen, generated on the surface of the steel due to cathodic reactions, diffuses into the atomic lattice, damaging the microstructure and degrading the mechanical properties. Atomic hydrogen can be generated during electroplating processes or when steel components are exposed to aqueous fluid in service. Therefore, the possibility of hydrogen embrittlement is an important issue when high strength steels are electroplated.

The process of SCC consists of cracking under the combined effect of a static tensile stress and corrosion in the absence of large scale plastic deformation. This is associated with three possible mechanisms: active path dissolution, film induced cracking and hydrogen embrittlement. The latter mechanism is the most likely for high strength steels.

A study has been conducted to clarify the properties of M54 and the effect of electroplating on the integrity of the steel substrate. The study results are compiled in this report.

---

*4340 steel, 300M steel, AerMet 100 steel, and Ferrium M54 steel are called simply as 4340, 300M, AerMet 100, and M54 in this report.

EXPERIMENTAL PROCEDURE

MATERIAL

A forged square bar of M54, 4 x 4 x 24 in., was supplied by Latrobe Specialty Metals Co., Latrobe, PA. The typical chemical composition of the steel is shown in Table B-1, and the microstructure in Figure A-1. The steel was heat-treated by Hercules Heat Treating Corp., Brooklyn, NY as follows: solution-treating at 1940^{o} F (1060^{o}C) for 60-90 min, oil quenching, freezing at -100^{o} F (-73^{o}C) for 1-3 hr, air warming, tempering at 960^{o}F (516^{o}C) for 10 hr, and air cooling.

Zn-Ni alloys are reported to produce the highest corrosion resistance of the electroplated Zn alloys, the corrosion resistance on steel increasing with Ni content up to 15 to 18% (reference 1). Beyond this range the alloy becomes more noble than steel and loses its sacrificial protection property. Therefore, Zn-14% Ni alloy was selected as the coating material.

SPECIMENS

The square bar steel was machined to the following specimen configurations:

- round tension test specimen of gage length 1 in. and diameter 0.25 in. in S-orientation for tension test (ASTM E8) and slow strain rate test (ASTM G129)

- hourglass specimen of minimum diameter 0.25 in. in S-orientation for stress-life fatigue test (ASTM E466)

- compact tension specimens, 2 in. wide and 1 in. thick, in S-L and L-S orientations for fracture toughness test (ASTM E399)

- compact tension specimens, 1 in. wide and 0.125 in. thick, in S-L & L-S orientations for fatigue crack growth test (ASTM E647)

- square bar specimen of 0.4 x 0.4 x 2.8 in. in S-L orientation with a Charpy notch at the mid-length for SCC test under four-point bending (ASTM F 1624)

- flat plate specimen of 4 x 4 x 1/8 in. for electrochemical polarization experiment

ELECTROCHEMICAL EXAMINATION

The electrochemical behavior of M54 was characterized by conducting a polarization experiment in aqueous 3.5% NaCl solution of pH 7.3. For this experiment, a specimen was mounted in a flat cell that exposed a circular 0.2 in^{2} area to the solution. Before the start of the polarization experiment, the specimen was allowed to freely corrode in the NaCl solution under open-circuit condition until a steady-state potential was reached. For the polarization experiment, the potential of the specimen with respect to the Saturated Calomel Electrode (SCE) was controlled

with a SI 1287 Potentiostat/Galvanostat from 100 mV below the free corrosion potential, while the current required to maintain the potential of the specimen was recorded. The corrosion current was estimated through linear polarization resistance measurements using scans from 100 mV below to 100mV above at a scan rate of 0.167 mV/s.

ZINC-NICKEL ALLOY PLATING

The Zn-14% Ni alloy plating was performed, following the alkaline LHE (low hydrogen embrittlement) Zn-Ni alloy plating process, DIPSOL IZ-C17+ (reference 2). This process is approved for U.S. Air Force Drawing 201027456 high strength steel applications, and meets Boeing BAC5637 and AMS 2417 specifications for low strength steel and other substrates. It also meets the requirements for a non-embrittling process per ASTM F519.

TESTS

TENSION TEST

A 20 kip (90 KN) capacity Interlaken closed-loop servo-hydraulic mechanical test machine was utilized for the tension test. The test was conducted with the tension test specimen in air, following the ASTM E 8 – 01, Standard Test Methods for Tension Testing of Metallic Materials. The tensile loading rate was 0.003 in/min (0.076 mm/min).

STRESS-LIFE FATIGUE TEST

This test was also carried out in the 20 kip (90 KN) capacity Interlaken test machine, employing hourglass specimens, under stress control in tension-tension cycling at stress ratio 0.1 and frequency 10 Hz in air and aqueous 3.5% NaCl solution of pH 7.3. This test followed the ASTM E 466 – 96, Standard Practice for Conducting Force Controlled Constant Amplitude Axial Fatigue Tests of Metallic Materials.

FATIGUE CRACK GROWTH TEST

A horizontal closed-loop servo-hydraulic mechanical test machine of 10 kip (45 KN) capacity was used for the Fatigue Crack Growth (FCG) test in air and aqueous 3.5% NaCl solution of pH 7.3. The fatigue crack growth test was performed under stress control in tension-tension cycling of frequency 10 Hz with a sinusoidal waveform and stress ratios 0.1 and 0.7 at room temperature. The fatigue loading procedure was K-decreasing or load shedding with K-gradient parameter C = -1 $in.^{-1}$ (-0.08 mm^{-1}) in the near threshold FCG regime and K-increasing in the Paris and rapid unstable crack growth regimes. Using the compliance technique, the fatigue crack length was continuously monitored with a laboratory computer system, interfaced with the test machine. This test followed the ASTM E 647– 00, Standard Test Method for Measurement of Fatigue Crack Growth Rates.

STRESS CORROSION CRACKING TESTS

Two test methods, rising step load (RSL) and slow strain rate (SSR), were used to quantify the degree of hydrogen embrittlement or stress corrosion cracking produced in bare and plated M54 specimens during exposure to aqueous 3.5% NaCl solution of pH 7.3.

RSL Test: Since the cantilever bend or double cantilever beam SCC test takes a long time, an accelerated SCC test was conducted in a RSL 1000 SI-Multi-Mode Test System (reference 3). This System included a bending frame, a tensile loading frame, an electrolyte reservoir, a pump for electrolyte circulation, a SCE, a platinum counter-electrode, a PC and a printer. The bare square bar specimens were precracked, whereas the plated ones were not. Subsequently, the specimens were step-loaded until the load dropped in four-point bending under constant displacement control, while held at a given potential in aqueous 3.5% NaCl solution of pH 7.3. The load drop corresponds to the threshold stress intensity for stress corrosion crack growth at a given cathodic potential.

SSR Test: The test was performed in a tensile loading frame at a strain rate, varying from 10^{-7} to 10^{-4} s^{-1}. The specimes were placed in an environmental chamber, which contained enough aqueous 3.5% NaCl solution of pH 7.3 to completely immerse the gage section of the specimen. During the test, the NaCl solution was continuously circulated between the environmental chamber and the reservoir by a pump. The specimens were pulled in tension to fracture, and the ultimate tensile strength (UTS) was recorded for comparison with the non-embrittled UTS of the test conducted in air.

FRACTOGRAPHY

After the stress-life fatigue and stress corrosion cracking tests, the morphology of the respective specimen fracture surfaces was examined with a JEOL JSM-6460LV scanning electron microscope, operated at an accelerating voltage of 20 kV.

EXPERIMENTAL RESULTS
PART I: BARE M54

ELECTROCHEMICAL CHARACTERISTICS

The results of the polarization experiment and open circuit potential (OCP) determination are shown in Figure A-2. The corrosion potential E or OCP and the corrosion current density i_{corr} of M54 were measured to be -0.55 volt and 10 $\mu A/cm^2$, respectively.

MECHANICAL PROPERTIES

The mechanical properties determined for M54 are UTS 298 ksi, YS 247 ksi, hardness Rockwell C 55, elongation 13%, K_{IC} 104 ksi$\sqrt{in}$ in L-S orientation and 95 ksi$\sqrt{in}$ in S-L orientation, and

K_{ISCC} 85 ksi√in in L-S orientation and 88 ksi√in in S-L orientation. These data are also shown in Table B-2 with those of 4340, 300M, AerMet 100 and Hy-Tuf.

FATIGUE BEHAVIOR

STRESS-LIFE FATIGUE

The stress-life fatigue curves are shown for the tests in air and aqueous 3.5% NaCl solution in Figure A-3. The fatigue strength was determined to be lower in the 3.5% NaCl solution than in air.

FRACTOGRAPHS FOR FATIGUE FRACTURE IN AIR

Typical SEM fractographs are shown in Figure A-4. They show:

- The fatigue crack was initiated at one of several cavities, connected or closely located, on the specimen surface. (a)
- In the vicinity of the crack initiation site, beach marks, secondary cracks along some beach marks, and cracks along some facet-boundaries are visible. (a)
- In the slow crack growth area, about 0.05 in. (1.3 mm) from the crack initiation site, well defined striations are seen in fatigue facets. Along some striations, secondary cracks can be found. (b)
- In the overload fracture area, about 1.2 in. (30 mm) from the crack initiation site, mostly equiaxed dimples of various sizes are noticeable. (c)

FRACTOGRAPHS FOR FATIGUE FRACTURE IN 3.5% NACL SOLUTION

Typical SEM fractographs are shown in Figure A-5. They show:

- The fatigue crack was initiated at a single site (a cavity) on the specimen surface. (a)
- In the vicinity of the crack initiation site, beach marks, striations, secondary cracks along some striations, and cracks along some facet-boundaries are noticeable. (a)
- In the slow crack growth area, striations and cracks along fatigue-facet boundaries are seen. (b)
- In the overload fracture area, about 0.13 in. (3.35 mm) from the crack initiation site, a mixture of scattered intergranular cracks and dimples is visible. (c)

FATIGUE CRACK GROWTH

Figures A-6 show the variation of fatigue crack growth rate da/dN with stress intensity range ΔK at stress ratios R=0.1 and 0.7 in air and aqueous 3.5% NaCl solution for the bare M54 specimens in S-L orientation. In air, the threshold stress intensity ranges ΔK_{th} for the fatigue crack growth at stress ratios R = 0.1 and 0.7 are 2.84 and 2.54 ksi√in, respectively. In aqueous 3.5% NaCl solution, the value of ΔK_{th} at R = 0.1 is 5.56 ksi√in. In both of the environments, the da/dN is greater for R = 0.7 within the range of employed ΔK values.

Figure A-7 shows the curves of da/dN vs ΔK in air and aqueous 3.5% NaCl solution for R = 0.1 and 0.7, indicating the environmental effect. The crack growth rate is lower in aqueous 3.5% NaCl solution than in air, indicating crack growth retardatation induced by corrosion product in aqueous 3.5% NaCl solution.

STRESS CORROSION CRACKING BEHAVIOR

RISING STEP LOAD TEST RESULT

The variation of threshold stress intensity for stress corrosion cracking, K_{ISCC}, and the net stress at failure, σ_{net}, with applied cathodic potential, V_{SCE}, is shown for the specimens of S-L orientation in Figure A-8. The K_{ISCC} and σ_{net} initially increased steeply from the minimum value at V_{SCE} = -1.2 volt, peaked at $V_{SCE} \cong$ -0.6 volt, and then decreased with increasing V_{SCE}. The K_{ISCC} value determined at -0.6 volt was 85 ksi√in for the L-S orientation, whereas it was 88 ksi√in for the S-L orientation. [As mentioned on page 4, the measured OCP is -0.55 volt.]

SLOW STRAIN RATE TEST RESULT

The variation of UTS with applied strain rate is shown for the tests in air and aqueous 3.5% NaCl solution in Figure A-9. This figure indicates that the UTS was nearly constant with respect to the changing strain rate in air, but smaller for the lower strain rate in the NaCl solution. At a strain rate of 10^{-7} s^{-1}, the UTS was reduced from 295 ksi in air to 215 ksi or 27% in the NaCl solution. The reduction in UTS is a quantitative measure of the SCC/hydrogen embrittlement that occurred in the NaCl solution.

PART II: COATED M54

COATING DEFECT

A Zn-14% Ni coated and baked specimen was cross-sectioned and examined for the presence of coating defects using optical microscopy. The micrographs, shown in Figure A-10, exhibit cavities, some along grain boundaries and some through-thickness, and intergranular cracking in the coating, and partial separation of the coating from the substrate. The through-thickness cavities and the partial separation of the coating leave the substrate exposed to the corrosive environment.

FATIGUE BEHAVIOR

STRESS-LIFE FATIGUE

The stress-life fatigue curves for the tests in air and aqueous 3.5% NaCl solution are shown in Figure A-11. The fatigue strength is lower in the NaCl solution than in air, especially at lower applied stresses.

FRACTOGRAPHS FOR FATIGUE FRACTURE IN AIR

Typical SEM fractographs are shown in Figure A-12. They show:

- In the vicinity of the crack initiation site, there is a short length where the coating is not adhered to the substrate, leaving a gap. The fatigue crack initiation site is located along the gap-boundary in the substrate (M54) side of the interface. Beach-marks are seen near the crack initiation site. (a)
- The slow crack growth area displays striations, secondary cracks along some striations, and cracks along some fatigue-facet boundaries. (b)
- In the overload fracture area, dimples of various sizes are visible. (c)

FRACTOGRAPHS FOR FATIGUE FRACTURE IN AQUEOUS 3.5% NaCl SOLUTION

Typical SEM fractographs are shown in Figure A-13. They show:

- In the vicinity of crack initiation site, separated grain facets are noticeable, scattered in the substrate side of the substrate/coating interface. The crack initiation site is located at a spot with separated grain facets. (a)
- The slow crack growth area displays striation-patches, secondary cracks along some striations, and cracks along some fatigue-facet boundaries. (b)
- In the overload fracture area, a mixture of dimples and separated grain facets is noticeable. (c)

STRESS CORROSION CRACKING BEHAVIOR

RISING STEP LOAD TEST RESULT

The variations of threshold stress intensity K_{ISCC} and net failure stress σ_{net} with applied cathodic potential V_{SCE} are shown for the specimens of S-L orientation in Figure A-14. Both K_{ISCC} and σ_{net} increased initially from the lowest values at V_{SCE} = -1.2 volt, peaked at $V_{SCE} \cong$ -0.9 volt for the coated specimen, and then decreased as the applied cathodic potential increased to -0.4 volt. The K_{ISCC} values of the coated specimen at V_{SCE} = -1.2, -0.9 and -0.4 volt are 40.7, 131.4 and 98.8 ksi$\sqrt{}$in., respectively.

FRACTOGRAPHS OF COATED M54 SCC-TESTED IN AQUEOUS 3.5% NaCl SOLUTION

Typical SEM fractographs are shown for V_{SCE} = -1.2 and -0.4 volt in Figure A-15. Intergranular cracking appears more clear-cut and extensive at V_{SCE} = -1.2 volt, shown in (a), than at V_{SCE} = -0.4 volt, shown in (b).

SLOW STRAIN RATE TEST RESULT

The variation of UTS with strain rate is shown for the coated specimens tested in air and 3.5% NaCl solution in Figure A-16. This figure indicates that the UTS is nearly constant with respect

to the strain rate in air, but it is smaller with lower strain rate in the NaCl solution. At the strain rate of 10^{-7} s^{-1}, the UTS is reduced from 296 ksi in air to 268 ksi or 9% in the NaCl solution.

DISCUSSION
PART I: BARE M54

FACTORS AFFECTING SCC SUSCEPTIBILITY

Yield strength and some alloying elements of a steel are known to affect its SCC susceptibility.

Yield strength: Shih and Clark (reference 4) showed that the SCC susceptibility of 4340 steel increases with an increase in yield strength level in sea water, distilled water and humid air.

C: Below 0.40%, K_{ISCC} increases with decreasing C concentration in 3.5% solution (reference 5).
P: The sulfide stress-corrosion cracking threshold stress is lower for a greater P concentration (reference 6).
Mn: K_{ISCC} decreases with increasing Mn concentration in 3.5% NaCl solution (reference 5).
V: V increases strength, hardness, creep-resistance and impact resistance due to formation of hard vanadium carbides and limits grain size (reference 7). Spencer and Duquette (reference 8) found that vanadium carbide (V_4C_3) in 4340 significantly decreases the hydrogen embrittlement/SCC susceptibility, because vanadium carbide traps ties up diffusible hydrogen.
W: W increases hardness, particularly at elevated temperatures, due to its stable carbide formed, and refines grain size (reference 7). It is not sure whether the tungsten carbide also traps hydrogen and reduces hydrogen embrittlement/SCC susceptibility, as vanadium carbide does.

On the other hand, some investigators reported that only Cr among the elements Ni, Cr, Mo, V, Mn Al, and N in HY-150 type steels has a greater effect on K_{ISCC} than on K_{IC} (reference 9-11).

The chemical composition of M54 is compared to those of some other high strength steels in Table B-1. M54 contains greater amount of Cr, Ni and Mo than are present in 4340 and 300M, but not as much as are present in AerMet 100. There is also less Co in M54 than in AerMet 100. On the other hand, M54 contains 0.10 % V and 1.30% W, elements that are not present in 4340, 300M and AerMet 100. The C concentration of M54 is slightly greater than that of AerMet 100, whereas it is less than those of 4340 and 300M. M54 and AerMet 100 contain little or no P, whereas 4340 and 300M contain some amount of P. M54 contains no Mn, whereas 4340, 300M and AerMet 100 contain some amount of Mn. This comparison of chemical compositions seems to indicate that the very high SCC resistance of M54 may be attributed to the extra alloying elements, V and W.

COMPARATIVE ELECTROCHEMICAL CHARACTERISTICS

Figure A-2 shows polarization curves for M54 in comparison with AerMet 100, 4340 and 300M. The corrosion potential or open circuit potential of M54 is less than that of AerMet 100, but it is greater than those of 4340 and 300M. In other words, M54 is more active (or more susceptible to

corrosion) than AerMet 100, and both 4340 and 300M are more active than M54. Apparently, the difference in activity is associated with the relative concentration of Cr, Ni and Co in these four steels, Table B-1.

MECHANICAL PROPERTIES

The mechanical properties of M54 are similar to those of AerMet 100, as shown in Table B-2.

FATIGUE BEHAVIOR

The fatigue strength of M54 is lower in aqueous 3.5% NaCl solution than in air, Figure A-3. This demonstrates the susceptibility of this steel to corrosion fatigue in the NaCl solution. The fatigue strength of M54 is compared to those of AerMet 100 (reference 12), 300M (reference 13), and 4340 (reference 12) in Figures A-17(b) and (c). In air and aqueous 3.5% NaCl solution, the fatigue strength of M54 steel in S-L orientation is close to those of the three steels in L-T orientation.

The fatigue crack growth rates of M54 in air and 3.5% NaCl are compared with those of AerMet 100, 300M, and 4340 (reference 12) in Figure A-18. In air, the threshold stress intensity range for fatigue crack growth ΔK_{th} of M54 is lower than those for AerMet 100 and 300M but close to that for 4340, Figure A-18(a). This indicates that M54 is more susceptible to threshold fatigue crack growth than AerMet 100 and 300M in air. However, the da/dN of M54 is similar to those of the other three steels in the greater ΔK region. On the other hand, in aqueous 3.5% NaCl solution, the ΔK_{th} of M54 is much greater than those of the other three steels, Figure A-18(b). This indicates that M54 has greater resistance to threshold fatigue crack growth than the other three steels in aqueous 3.5% NaCl solution. The greater value of ΔK_{th} for M54 in comparison with the three other steels in aqueous 3.5% NaCl solution may be associated with the extra alloying elements in M54, V and W.

SCC RESISTANCE DETERMINED BY SLOW STRAIN RATE METHOD

The nearly constant UTS in the range of strain rate from $1x10^{-4}$ to $1x10^{-7}$ s^{-1} in air , noticeable in the plot of UTS vs. strain rate (Figure A-9), evidences no detectable SCC/hydrogen embrittlement occurring in M54 under slow straining in air.

The UTS reduction from 295 ksi in air to 215 ksi in aqueous 3.5% NaCl solution at strain rate $1x10^{-7}$ s^{-1}, Figure A-9, is attributable to the SCC/hydrogen embrittlement induced by slow straining in the corrosive environment (references 14, 15, and 16).

To assess the extent of SCC/hydrogen embrittlement, a susceptibility index I_{stress} is defined as follows (references 17 and 18).

$$I_{stress} = 1 - (S_{NaCl} / S_{air}) = \Delta S/S_{air} \quad (1)$$

where S_{NaCl} and S_{air} are the UTS values measured in aqueous 3.5% NaCl solution and air, respectively, for a given applied strain rate, and $\Delta S = S_{air} - S_{Nacl}$.

For the strain rate of 10^{-7} s^{-1} applied, the I_{stress} of M54 was calculated to be 0.27. Generally, I_{stress} values greater than 0.60 are taken to indicate severe SCC/hydrogen embrittlement (reference 17).

On the change of SCC/hydrogen embrittlement susceptibility with strain rate, it has been suggested that at high strain rate, the corrosion process cannot keep up with the strain process, and the influence of corrosion is negligible (reference 19). With decreasing strain rate, the latter influence becomes more significant. The attack by the corrosive environment reaches a maximum at a strain rate where the repassivation or oxide film formation can overtake the activation caused by the straining. The formation of oxide film on a metal surface reduces the reactivity of the underlying metal, and its rupture must occur before a crack can be initiated. According to the film-rupture theory, rupture takes place during straining by slip-steps emerging at the surface, and localized corrosion and/or anodic dissolution then occurs at the small area of freshly exposed metal to initiate a crack (reference 20). On further decrease of the strain rate, active sites are repassivated or filmed with oxide before a corrosion attack can take place. This results in a reduction of SCC/hydrogen embrittlement susceptibility.

PART II: COATED M54

FATIGUE BEHAVIOR

The fatigue strength of a coated specimen is lower in aqueous 3.5% NaCl solution than in air, Figure A-19(a). This demonstrates that the coated steel is also susceptible to corrosion fatigue in the NaCl solution. The fatigue strengths of the bare and Zn-14% Ni coated specimens are compared in air and aqueous 3.5% NaCl solution in Figures A-19(b) and (c).

In air, the fatigue strength of the coated specimen is lower than that of the bare one, Figure A-19(b). This behavior has also been reported for other steels. The fatigue strength of Cd-coated Hy-Tuf was lower than that of the bare steel in air (reference 21). Similarly, the lower fatigue strength in air was observed for the 4340, which was subjected to the following three coating systems (reference 22). Those systems were:

No. 1: Electroplated cadmium, hydrogen embrittlement relief treatment and chromate passivation
No. 2: No. 1 coating system and chromated epoxy primer
No. 3: No. 2 coating system and gloss white polyurethane topcoat

The reduction of fatigue strength in coated samples in air was attributed to hydrogen embrittlement, induced during the Cd-electroplating process (reference 22). The inferior fatigue strength of the coated M54 in air may also be caused by possible hydrogen embrittlement, induced during the process of Zn-14% Ni alloy electroplating.

In 3.5% NaCl solution, the fatigue strength of M54 is greater when coated than when bare, Figure A-19(c). The greater fatigue strength of the coated steel in aqueous 3.5% NaCl solution

must be attributed to the protective action of the Zn-14% Ni alloy coating against corrosion fatigue cracking.

SCC/HYDROGEN EMBRITTLEMENT

The coating porosity, similar to that observed in this study (Figure A-10), was also observed by Figueroa and Robinson (reference 16) in the coatings of Cd, Zn-14% Ni and SermeTel 1140/962. The observed cavities, especially those through-thickness, are attributable to hydrogen bubble formation during electroplating (reference 16). The exposed areas of the substrate would be preferential sites for hydrogen uptake.

The results of rising step load tests for bare and coated M54 are compared in Figure A-20, which shows the variations of threshold stress intensity vs. applied cathodic potential for bare & coated M54 specimens. The K_{ISCC} and net stress values are greater for coated specimen than for bare one at a given cathodic potential. The following are considered to be potential explanation: (1) The coated specimens were not precracked , whereas the bare ones were precracked. As the result, the stress concentration factor K_t was mnch greater for the bare specimens. (2) The substrate of the coated specimen can be protected (or insulated) from the corrosive environment during RSL test in aqueous 3.5% NaCl solution.

The coated steel can also be embrittled by the hydrogen, generated during corrosion of the sacrificial coating in a corrosive environment. In such a case, the hydrogen diffuses into the substrate and reaches a sufficient concentration for a crack to initiate. The extent of embrittlement depends on several factors: the electrochemical potential of the coating and the resulting couple potential with the steel (reference 17); the presence of through-the-thickness flaws in the coating, which leave areas of steel exposed (reference 23); hydrogen transport and trapping within the steel (reference 23); the susceptibility of the microstructure to crack initiation and propagation (reference 24).

In this study, no reduction in UTS was detectable during the slow strain rate loading of coated specimens in air, Figure A-16(b). This is evidences that there was no residual hydrogen embrittlement/SCC of the coated specimen.

On the other hand, the UTS reduction in 3.5% NaCl solution was 9% under slow strain rate loading for the coated specimen, Figure A-16(b), whereas that for the bare one was 27%, Figure A-16(a). The embrittlement indexes I_{stress} calculated from the UTS reduction are 0.094 for the coated specimen and 0.27 for the bare one at a strain rate of 10^{-7} s^{-1}. The smaller embrittlement index of the coated specimen indicates the extent of the protection of the substrate against SCC/hydrogen embrittlement by the Zn-14% Ni alloy coating in the corrosive environment.

Figure A-21 shows the variation of K_{ISCC} with V_{SCE} found for M54 (Figure A-8) and the high strength steels, AerMet 100 (reference 6), 300M (reference 25) and 4340 (reference 26). From this figure, it is clear that the K_{ISCC} of M54 is greater than those of the others' in the region of the V_{SCE} greater than -1 volt. In particular, the peak K_{ISCC} value of M54 is about four times greater than those of the other three steels. In other words, the SCC resistance of M54, measured by the

rising step load method, is far greater than those of the other high strength steels. A greater SCC resistance implies a greater resistance to a sustained or slow tension and intergranular cracking in a corrosive environment. The enhanced resistance may be attributable to the presence of the extra alloying elements, V and W, in M54. This remains to be studied further and clarified.

The K_{ISCC} value of M54 at V_{SCE} = -0.6 volt determined in this study, 88 ksi√in., is less than that determined by Sebastian of QuesTek Innovations LLC , 106 ksi√in. (reference 27).

FRACTOGRAPHIC FEATURES FOR BARE & COATED SPECIMENS

For the both bare and coated M54 specimens, the difference in fractographic features is the absence of intergranularly separated grain facets for the fatigue test in air and their presence for samples tested in 3.5% NaCl solution, Figures A-4, A-5, A-12, and A-13. The presence of the separated grain facets implies the occurrence of intergranular cracking/stress corrosion cracking during corrosion fatigue crack growth. Therefore, the mechanism of fatigue crack growth is striation formation in air and a combination of striation formation and intergranular cracking in 3.5% NaCl solution. A similar fractographic feature (a mixture of fatigue striations and intergranular cracking) was also reported for a 7075-T651 aluminum alloy, which was subjected to biaxial fatigue loading in 3.5% NaCl solution (reference 27).

CONCLUSIONS

- The open circuit potential of M54 is -0.55 volt, which is less than that of AerMet 100 but greater than those of 4340 and 300M in aqueous 3.5% NaCl solution of pH 7.3.

- The threshold stress intensity for stress corrosion cracking K_{ISCC} of M54 is far greater (by about four times) than those of 4340, 300M, and AerMet 100 in aqueous 3.5% NaCl solution. However, M54 is still susceptible to corrosion fatigue as 4340 and AerMet 100 are in aqueous 3.5% NaCl solution.

- The greater ΔK_{th} value and SCC resistance of M54 in aqueous 3.5% NaCl solution may be associated with its extra alloying elements, V and W, which are not present in AerMet 100, 300M and 4340.

- Zn-14% Ni alloy coating can provide M54 a certain degree of protection from stress corrosion cracking and corrosion fatigue in aqueous 3.5% NaCl solution.

- The mechanism of fatigue crack growth is striation formation in air and a combination of striation formation and intergranualar cracking in aqueous 3.5% NaCl solution for both of the bare and Zn-14% alloy coated M54.

RECOMMENDATIONS

Further investigate the following:

- The stress corrosion cracking behavior of M54 steel to establish the mechanism of high SCC resistance
- The corrosion fatigue resistance of M54 in order to enhance it.

REFERENCES

1. Nabil Zaki, "Zinc Alloy Plating," in *ASM Handbook, Vol. 5, Surface Engineering*, ASM International, 1994, pp. 264-265.

2. Technical Bulletin, DIPSOL of America, Inc., Livonia, MI, of 1 Jun 2013.

3. Rising Step-Load Test, ASM Handbook, Vol. 8, Mechanical Testing, ASM International, Jun 1995, pp. 539-40.

4. T. T. Shih and W. G. Clark, Jr., "An Evaluation of Environment-Enhanced Fatigue Crack Growth Rate Testing as an Accelerated Static Load Corrosion Test, in Environment-Sensitive Fracture, S. W. Dean, E. N. Pigh and G. M. Ugiansky, Ed., STP 821, American Society for Testing and Materials, Philadelphia, 1984, pp. 325-340.

5. Stress Corrosion Cracking and Hydrogen Embrittlement of Iron Base Alloys, NACE 5, National Association of Corrosion Engineers, Houston, 1974.

6. H. Asahi, "Effects of Mn, P, and Mo on Sulfide Stress Corrosion Cracking Resistance of High Strength Low Alloy Steels, Met. Trans. A, Vol. 19A, 1988, pp. 2171-2178.

7. Metals Handbook, Vol. 1, 10^{th} Edition, Properties and Selection: Iron, Steels, and High-Performance Alloys, ASM International, 1990, p. 395.

8. G. L. Spencer and D. J. Duquette, "The Role of Vanadium Carbide Traps in Reducing The Hydrogen Embrittlement Susceptibility of High Strength Alloy Steels," Technical Report ARCCB-TR-98016, US Army Armament Research Development and Engineering Center, Watervliet, N. Y. 12189-4050, Aug 1998. [Hydrogen is supplied as molecular gas, through stress corrosion, or by electrolytic charging.]

9. L. P. Connor, L. F. Porter, and S. T. Rolfe, *Fourth Progress Report: Extended Investigation of HY 130/150 Weldments,* U. S. Steel Corp., Monroeville, PA, of 1 Jul 1968, AD835687.

10. L. P. Connor, L. F. Porter, and S. T. Rolfe, *Fifth Progress Report: Extended Investigation of HY 130/150 Weldments,* U. S. Steel Corp., Monroeville, PA, of 2 Jan 1969, AD846122.

11. J. H. Smith and S. T. Rolfe, *Effect of Composition on the K_{ISCC} of Experimental HY-150 Steels,* U. S. Steel Corp., Monroeville, PA, of 20 Dec 1968, AD846121.

12. NAWCAD Report No. NAWCADPAX/TR-2009/12, "Aircraft Steels," E. U. Lee, R. Taylor, C. Lei and H. C. Sanders, of 19 Feb 2009.

13. Report AFML F33615-69-C-1115, "Mechanical Property Data 300M Steel," O. Deel, of Dec 1969.

14. W. J. Pollock: in *Hydrogen Embrittlement: Prevention and Control,* ASTM STP 962, L. Raymond, Ed., American Society for Testing and Materials, Philadelphia, 1988, pp. 68-80.

15. W. J. Pollock and C. Grey: in *Hydrogen Embrittlement: Prevention and Control,* ASTM STP 962, L. Raymond, Ed., American Society for Testing and Materials, Philadelphia, 1988, pp. 372-386.

16. D. Figueroa and M. J. Robinson, *Corrosion Science,* 2008, Vol. 50, pp. 1066-1079.

17. E. M. K. Hiller and M. J. Robinson, *Corrosion Science,* 2004, Vol. 46, pp. 715-727.

18. NAWCAD Report No. NAWCADPAX/TR-2012/206, "Stress Corrosion Cracking of Aluminum Alloys," E. U. Lee, R. Taylor, C. Lei, B. Pregger and E. Lipnickas, of 10 Sep 2012.

19. H. Buhl: in *Stress Corrosion Cracking – The Slow Strain Rate Technique,* G. M. Ugiansky and J. H. Payer, eds., ASTM STP 665, ASTM, Philadelphia, PA, 1979, pp. 333-346.

20. C. D. Kim and R. F. Wilde: in *The Slow Strain Rate Technique,* G. M. Ugiansky and J. H. Payer, eds., ASTM STP 665, ASTM, Philadelphia, P, 1979, pp. 97-112.

21. NAWCAD Report No. NAWCADPAX/TR-2005/20, "Study on Cadmium Replacement for Hy-Tuf Steel," E. U. Lee, H. C. Sanders, C. Lei and M. Yu, of 9 Mar 2005.

22. NAWCAD Report No. NAWCADPAX/TR-2013/252, "Coated 4340 Steel," E. U. Lee, C. Lei, M. Stanley, B. Pregger, and C. Matzdorf, of 26 Aug 2013.

23. H. E. Townsend, Jr., *Metallurgical Transactions A,* 1975, Vol. 6A, pp. 877-883.

24. NAWCAD Report No. NAWCADPAX/TR-2013/32, "Biaxial Fatigue Cracking from Notch," Eun U. Lee, Robert E. Taylor, Bruce A. Pregger, and Charles Lei, of 4 Mar 2013.

25. Eun U. Lee, Henry Sanders and Bhaskar Sarkar, "*Stress Corrosion Cracking of High Strength Steels,"* Proceedings of 1999 Tri-Service Conference on Corrosion, of 15-19 Nov 1999, Myrtle Beach, SC, Paper S08P2A.

26. Eun U. Lee, Amy Hilgeman, Erin Beck, Steve Brown and Craig Matzdorf, "*Cadmium Alternative Coating Corrosion Performance on 4340 Steel,"* Proceedings of 2007 Tri-Service Corrosion Conference, of 3-7 Dec 2007, Denver, Colorado, Paper P1792.

27. J. Sebastian: *NAVAIR SBIR (Contract N68335-08-C-0288) Phase II Final Report,* "Computational Design of Advanced Alloys for USN Landing Gear," of 10 May 2011, p. 28.

APPENDIX A
FIGURES

List of Figures

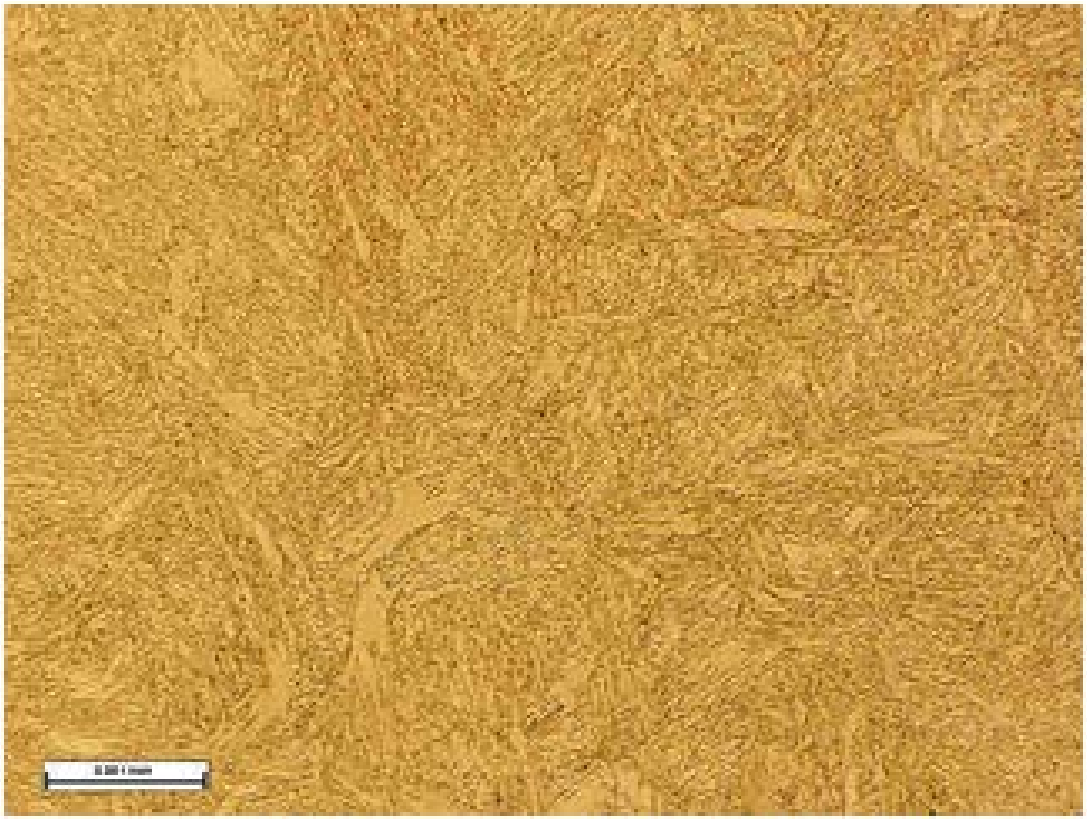

Figure A-1: Microstructure of Ferrium M54 Steel

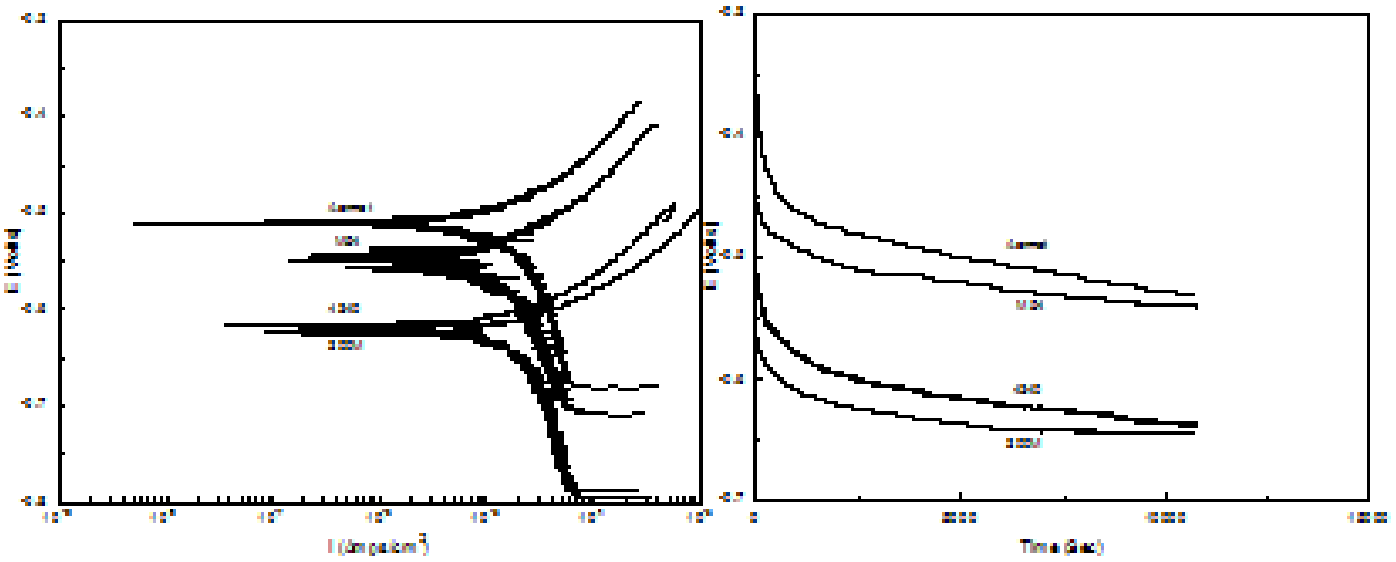

Figure A-2: Polarization and Open Circuit Potential Curves for M54, AerMet 100, 300M and 4340 Steels

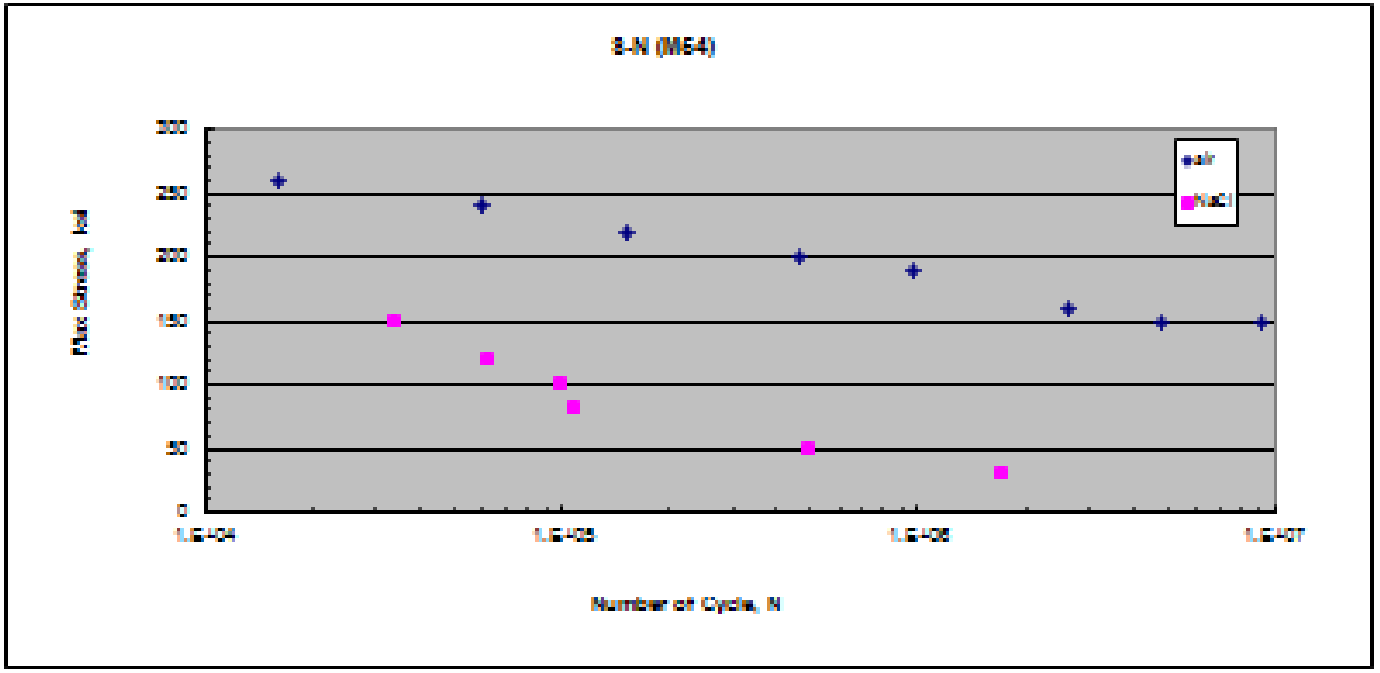

Figure A-3: Stress-Life Fatigue Curves for Bare Ferrium M54 Steel in Air & 3.5% NaCl Solution

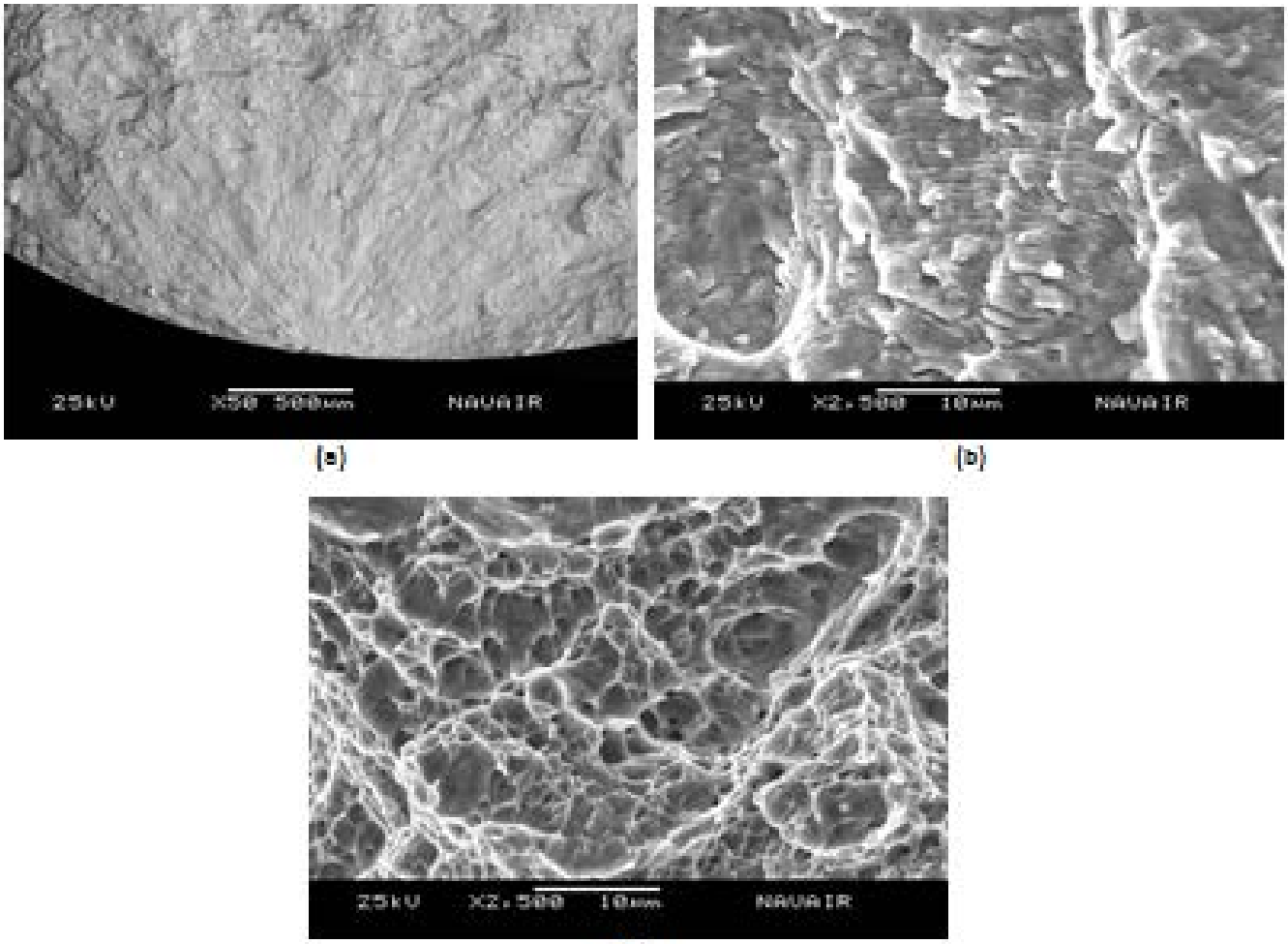

(a) (b)

(c)

Figure A-4: SEM Fractographs of Bare Ferrium M54 Steel Fatigue-Tested in Air

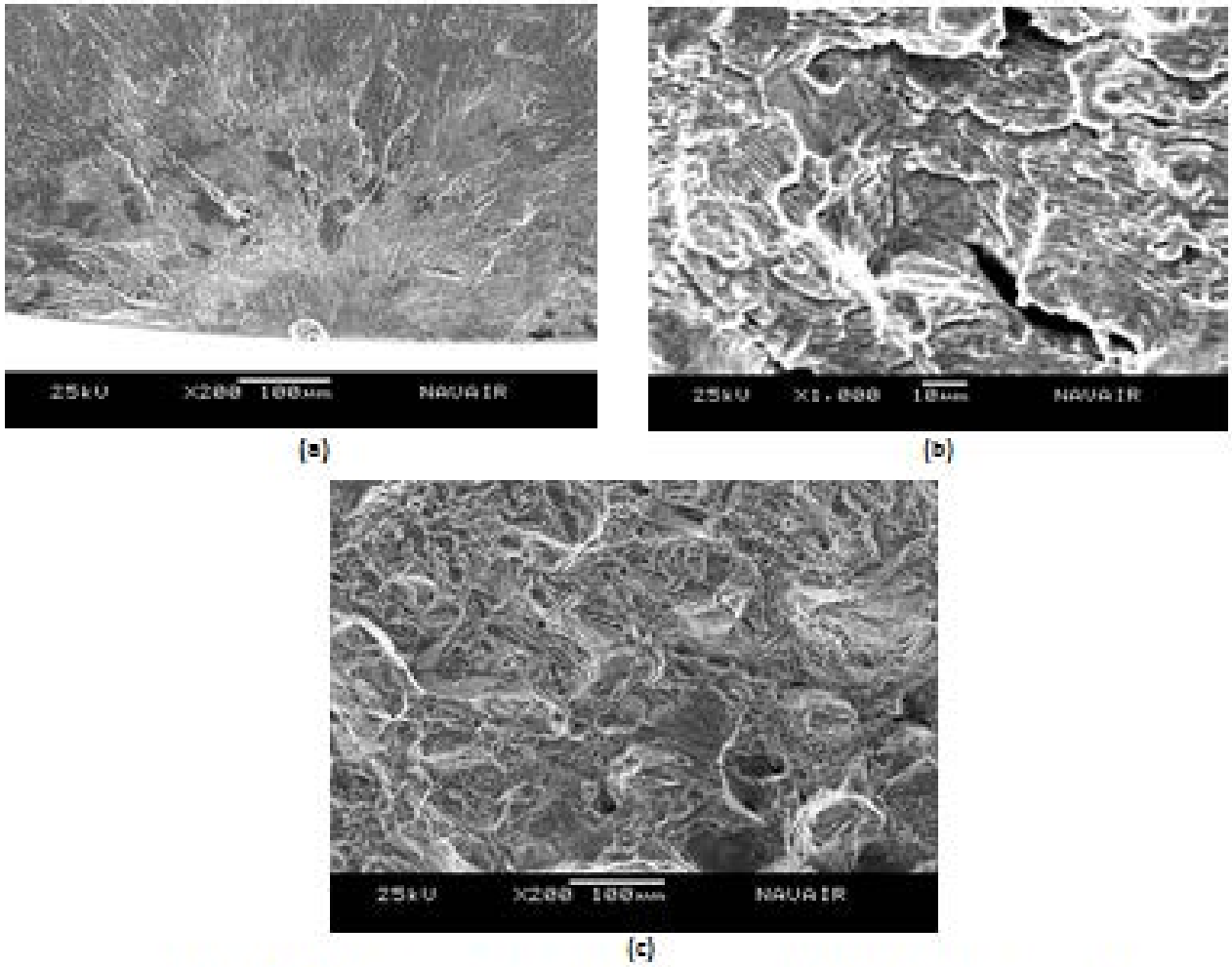

Figure A-5: SEM Fractographs of Bare Ferrium M54 Steel Fatigue-Tested in 3.5% NaCl Solution

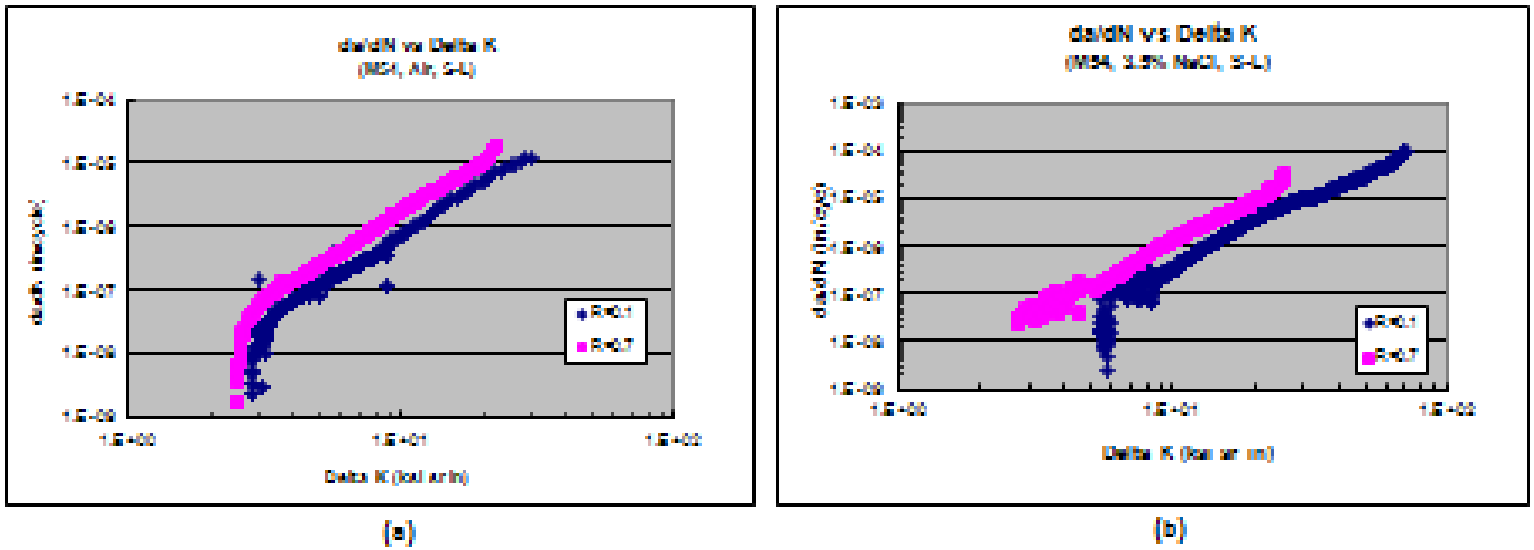

Figure A-6: da/dN vs. ΔK Curves for Bare Ferrium M54 Steel of S-L Orientation in Air & 3.5% NaCl Solution, Showing Stress Ratio Effect

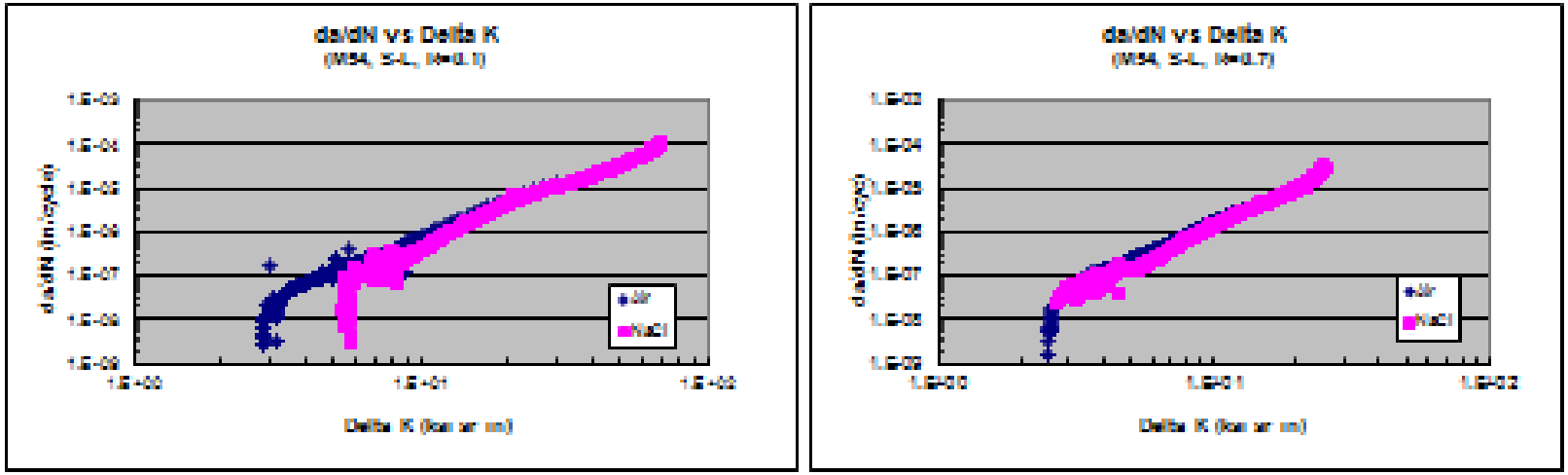

(a) (b)

Figure A-7: da/dN vs. ΔK Curves for Bare Ferrium M54 Steel of S-L Orientation at Stress Ratios 0.1 & 0.7, Showing Environmental Effect

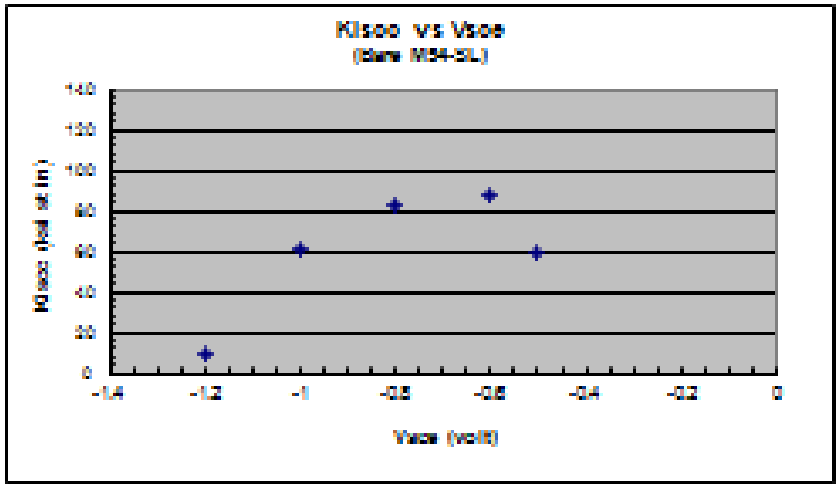

(a)

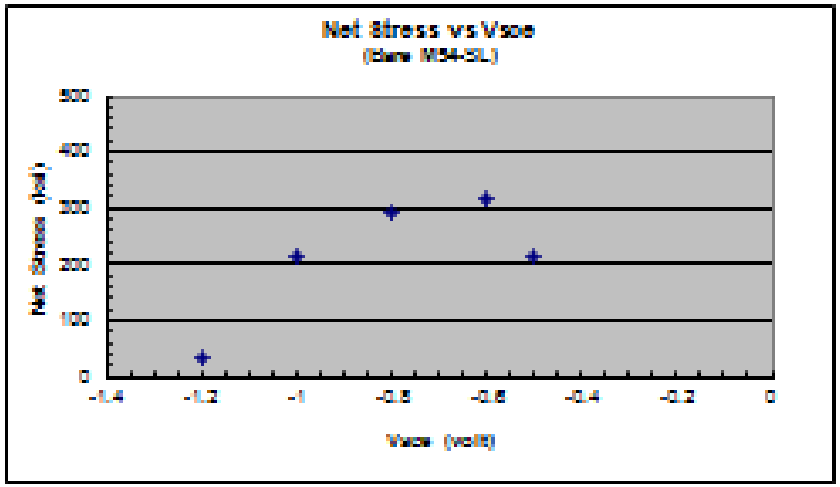

(b)

Figure A-8: Variation of K_{ISCC} & Net Stress at Failure with V_{SCE} for Bare Ferrium M54 Steel

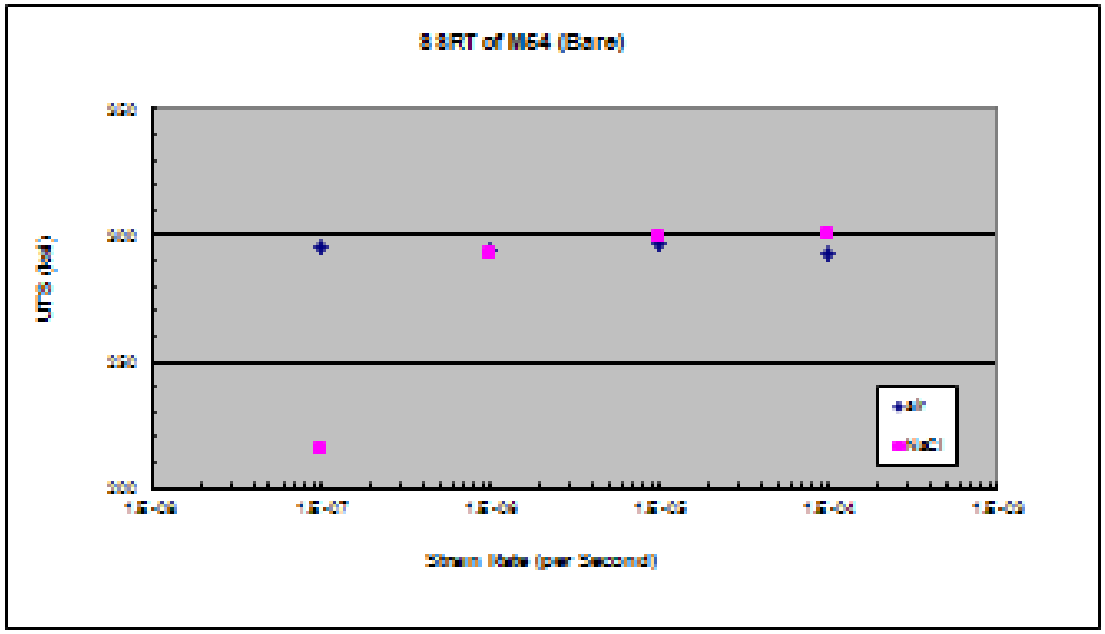

Figure A-9: Variation of UTS with Strain Rate for Bare Ferrium M54 Steel in Air & 3.5% NaCl Solution

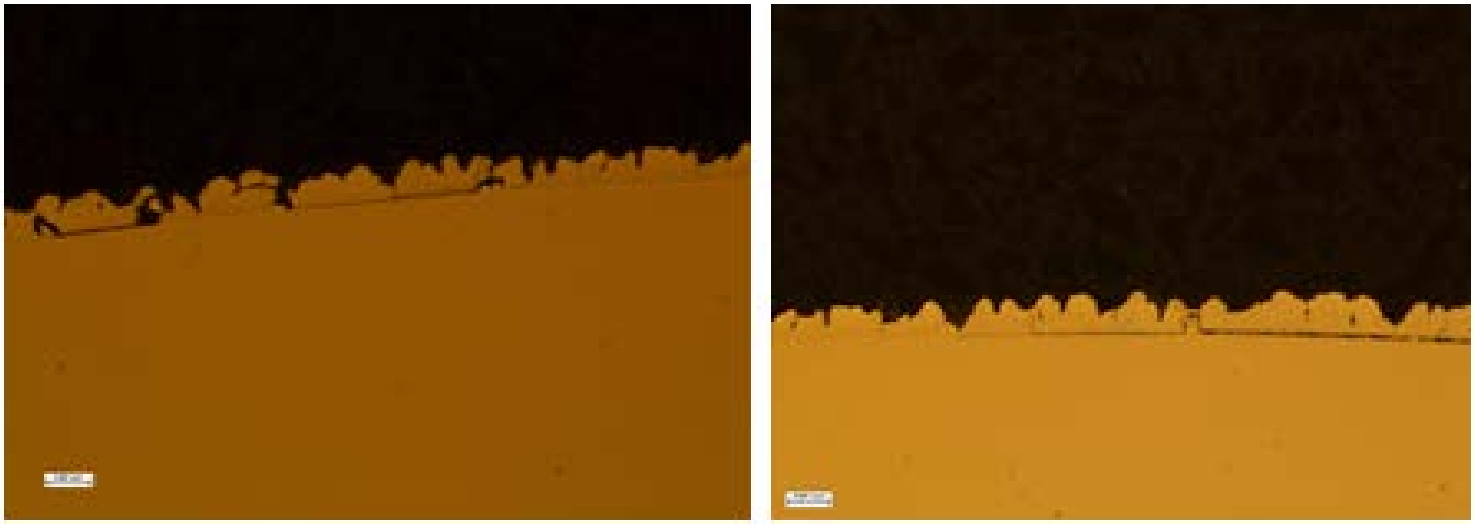

Figure A-10: Cross-Section of Coated & Baked Specimen

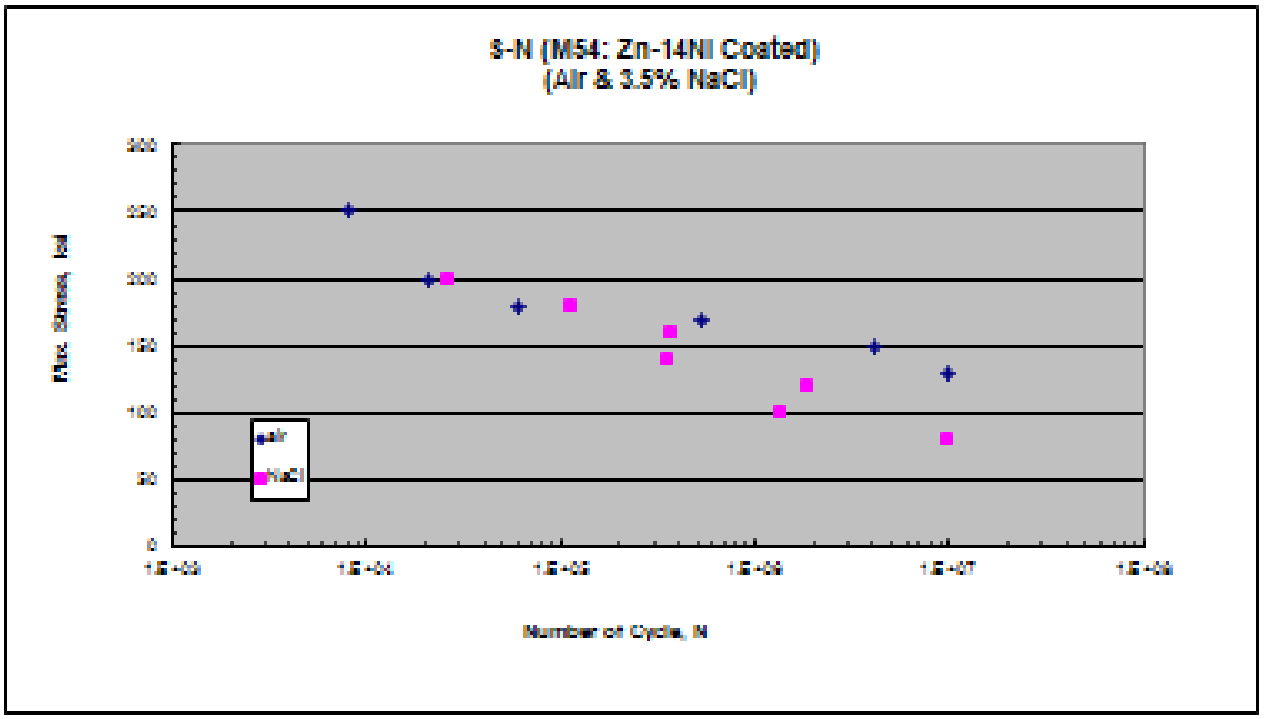

Figure A-11: Stress-Life Fatigue Curves for Coated Ferrium M54 Steel in Air & 3.5% NaCl Solution

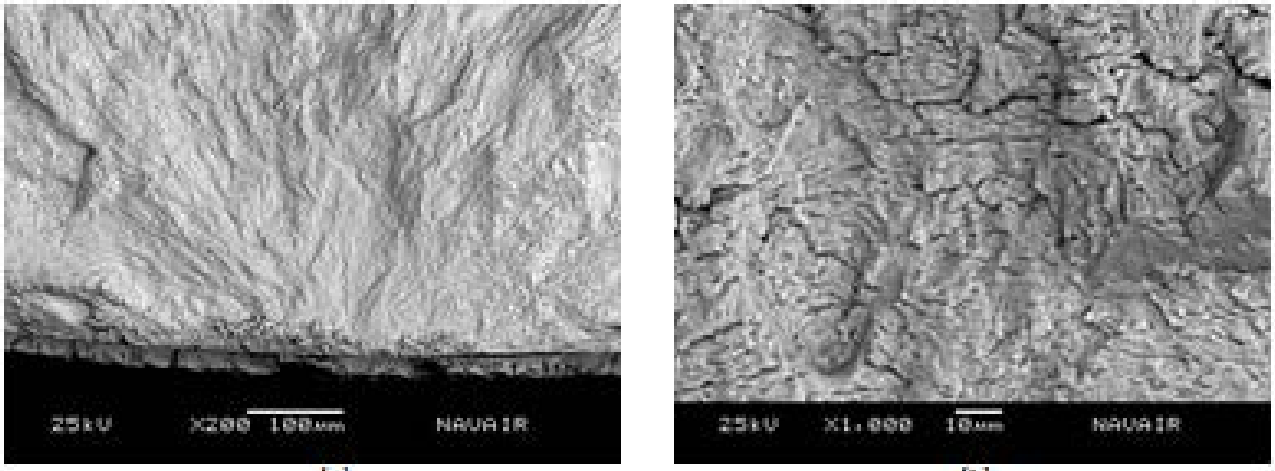

Figure A-12: SEM Fractographs of Coated Ferrium M54 Steel Fatigue-Tested in Air

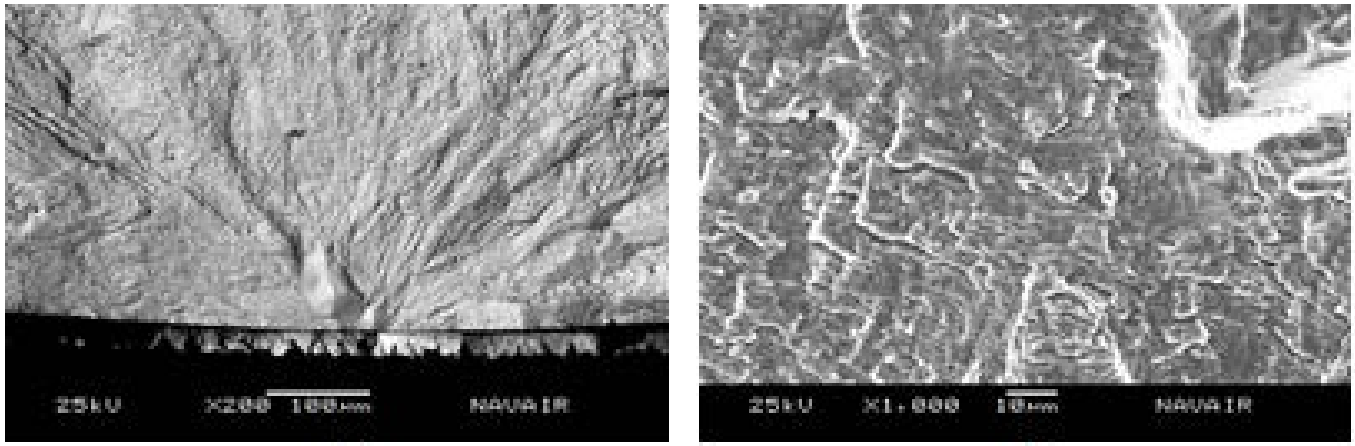

Figure A-13: SEM Fractographs of Coated Ferrium M54 Steel Fatigue-Tested in 3.5% NaCl Solution

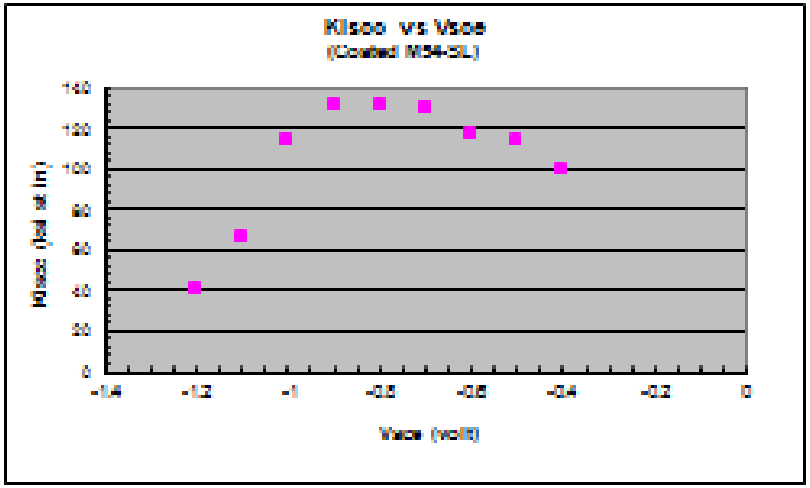

(a)

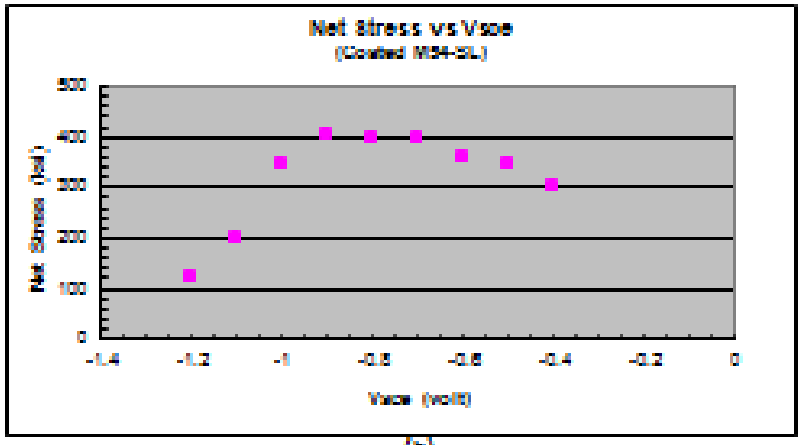

(b)

Figure A-14: Variation of K_{ISCC} & Net Stress at Failure with V_{SCE} for Coated Ferrium M54 Steel

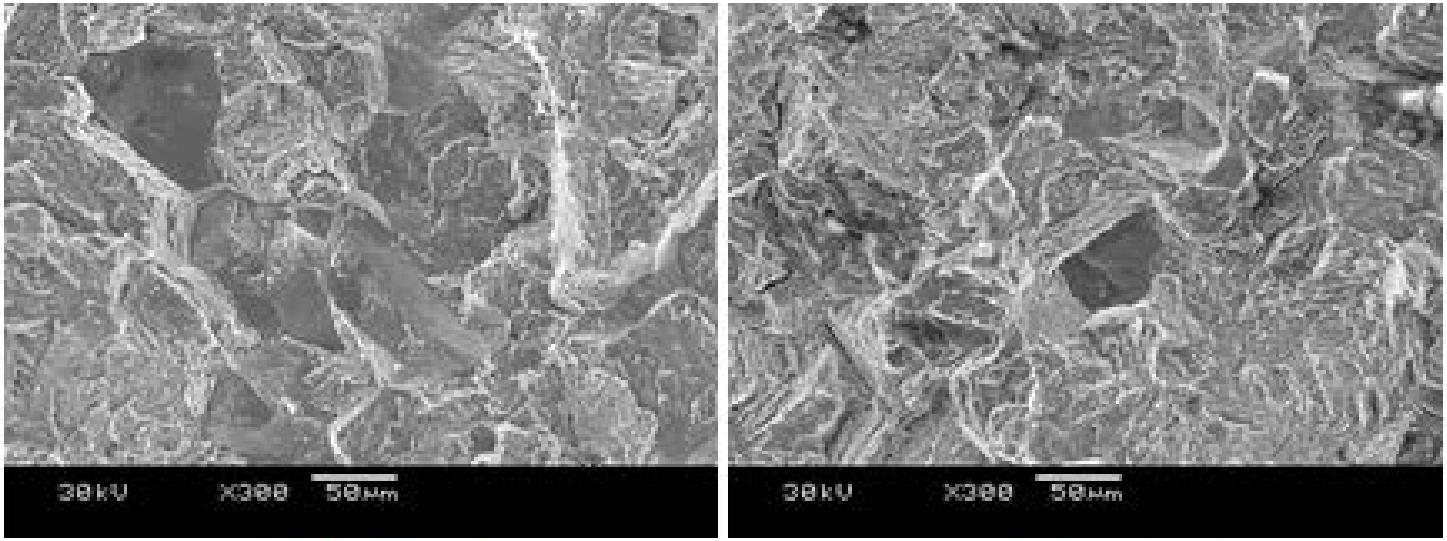

(a) V_{sce} = -1.2 volt (b) V_{sce} = -0.4 volt

Figure A-15: SEM Fractographs of Coated Ferrium M54 Steel RSL-SCC-Tested at Vsce = -1.2 & -0.4 volt in 3.5% NaCl Solution

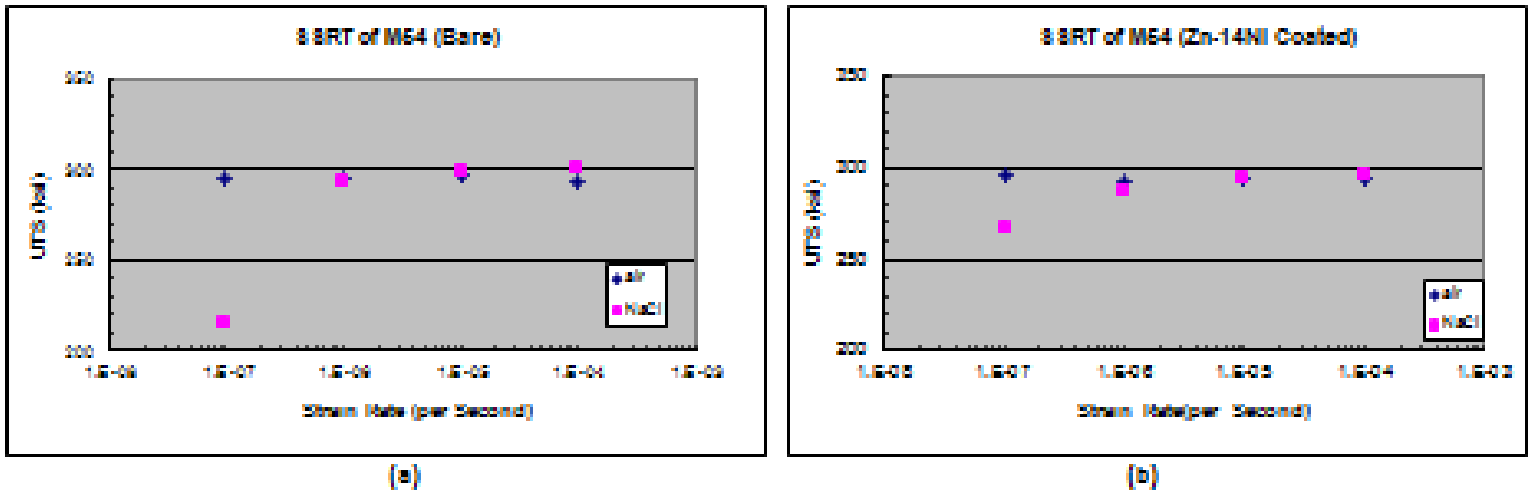

Figure A-16: Variation of UTS with Strain Rate for Bare & Coated M54 Steel in Air & 3.5% NaCl Solution

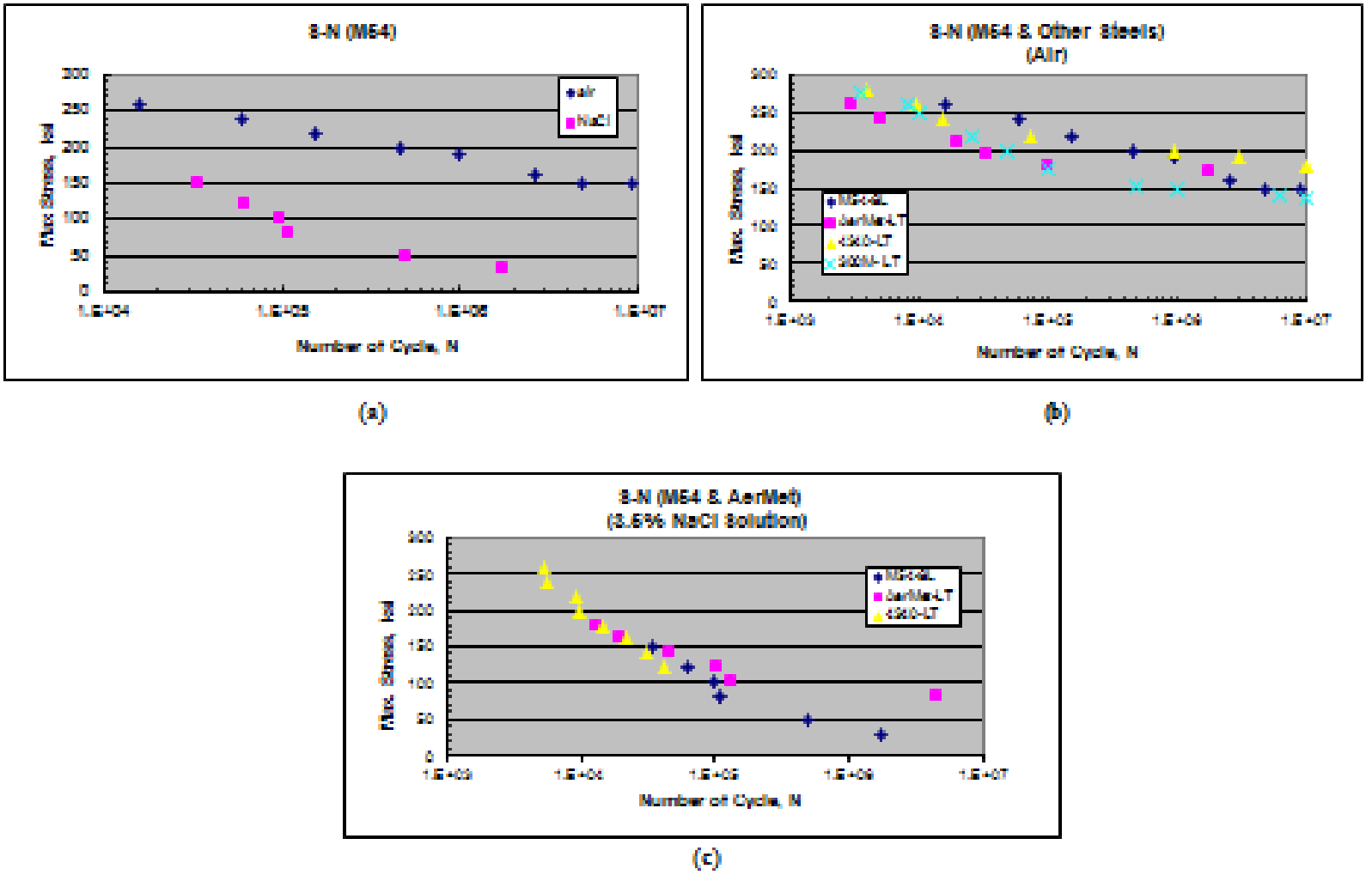

Figure A-17: Stress-Life Fatigue Curves for Bare Ferrium M54 & Other Steels

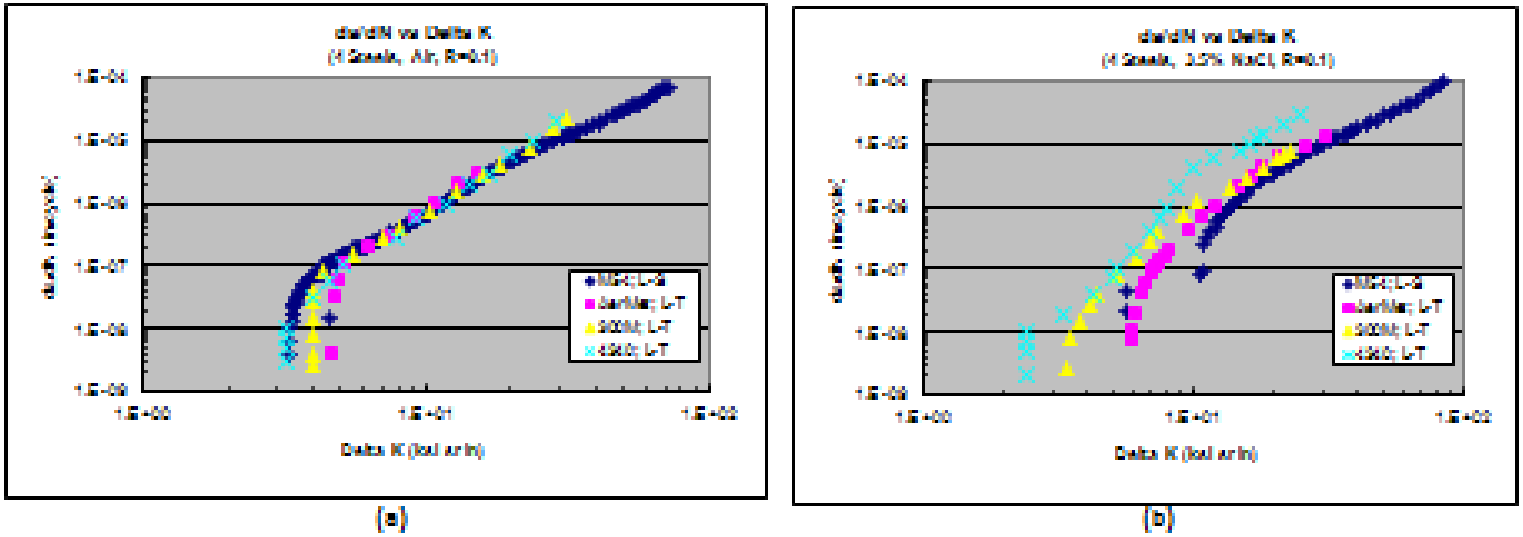

Figure A-18: Comparison of FCG Rates of Bare Ferrium M54 & Other Steels in Air & 3.5% NaCl Solution

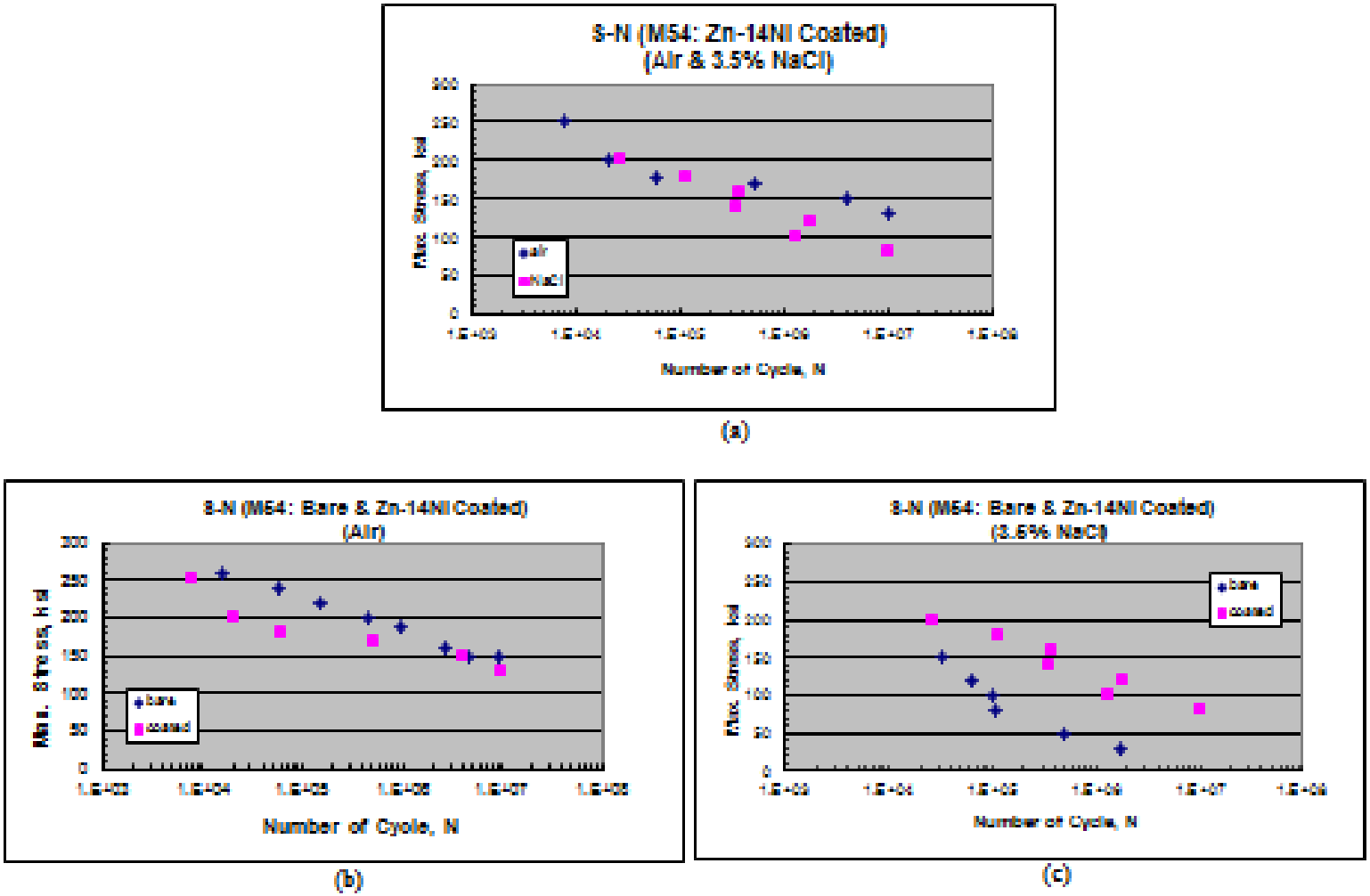

Figure A-19: Stress-Life Fatigue Curves for Coated Ferrium M54 Steel in Air & 3.5% NaCl Solution

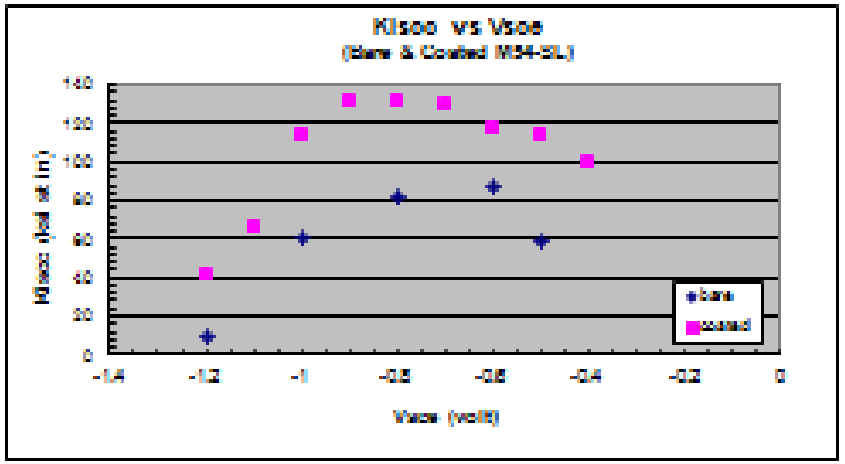

(a)

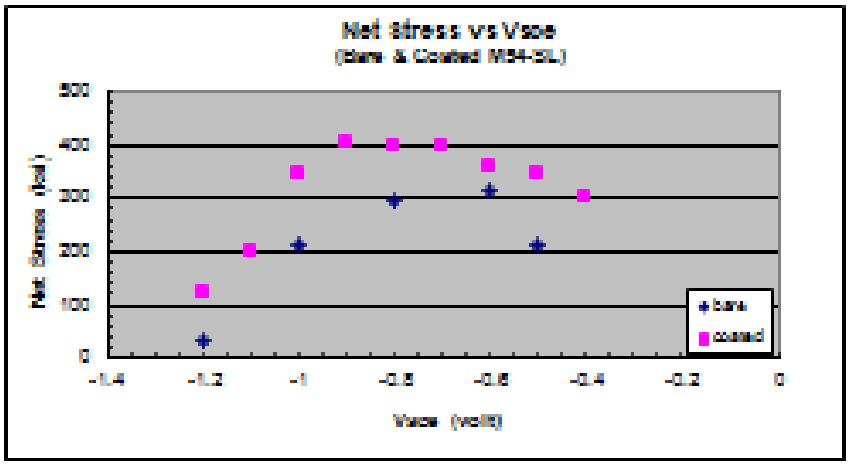

(b)

Figure A-20: Variation of K_{ISCC} & Net Stress at Failure with V_{SCE} for Bare & Coated Ferrium M54 Steel

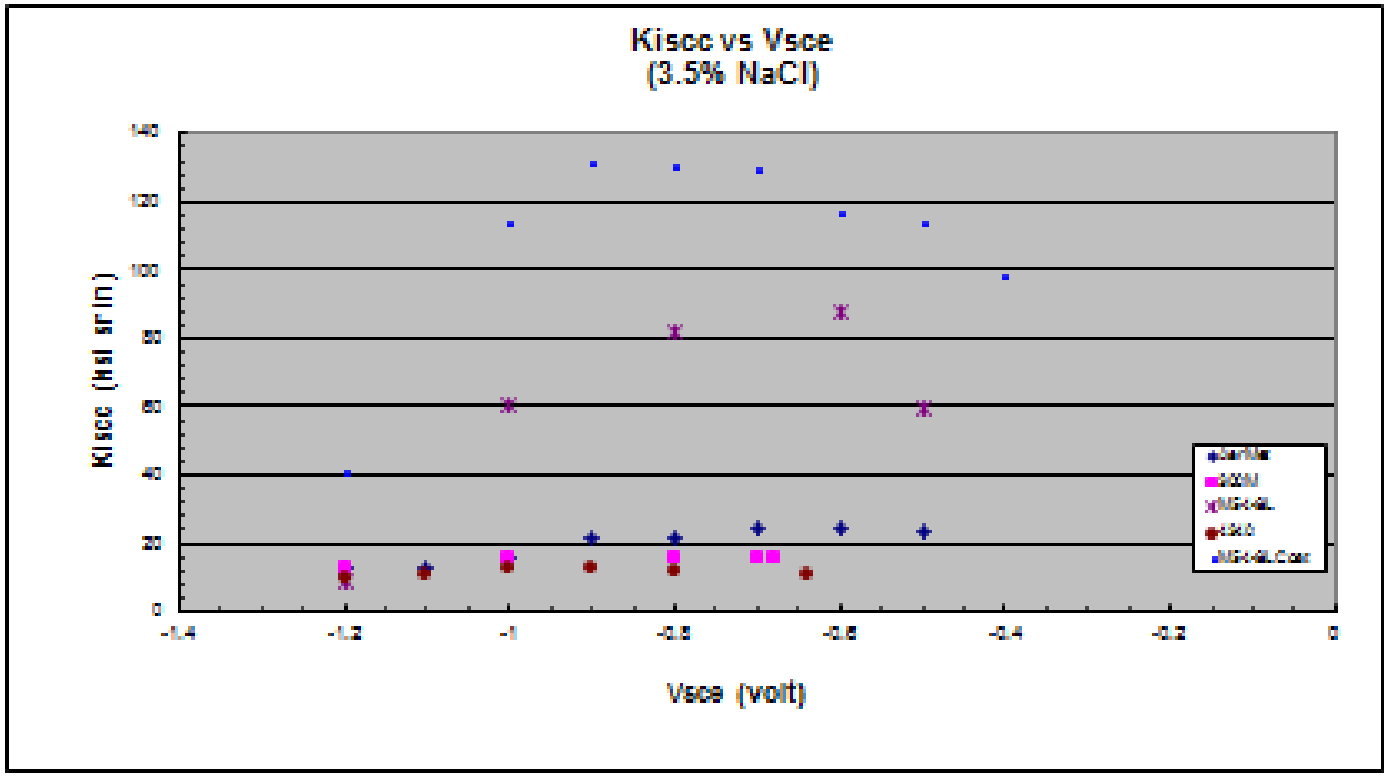

Figure A-21: Variation of K_{ISCC} with V_{SCE} for Bare & Coated Ferrium M54 & Other Bare Steels

APPENDIX B
TABLES

Table B-1: Chemical Compositions of Ferrium M54 and Other Steels

Chemical Composition of High Strength Steels					
	Composition (wt %)				
Element	**4340**	**300M**	**AerMet**	**M54**	**Hy-Tuf**
C	0.38 - 0.43	0.38 - 0.43	0.23	0.30	0.25
Mn	0.60 - 0.90	0.60 - 0.90	0.03	-	1.35
Si	0.15 - 0.35	1.45 - 1.80	0.03	-	1.50
P	0.015 max	0.010 max	0.00	-	-
Si	0.015 max	0.010 max	0.00	-	-
Cr	0.70 - 0.90	0.70 - 0.95	3.03	1.00	0.30
Ni	1.65 - 2.00	1.65 - 2.00	11.09	10.00	1.80
Mo	0.20 - 0.30	0.30 - 0.50	1.18	2.00	0.40
Cu	0.35 max	0.35 max	-	-	0.01
Co	-	-	13.44	7.00	-
V	-	-	-	0.10	0.29
W	-	-	-	1.30	-
Fe	balance	balance	balance	balance	balance

Table B-2: Mechanical Properties of Ferrium M54 and Other Steels

Mechanical Properties of High Strength Steels					
Property	**4340**	**300M**	**AerMet**	**M54**	**Hy-Tuf**
UTS (ksi)	282	290	294	298	235
YS (ksi)	242	245	248	247	187
Hardness (HRC)	51	54	53	55	47
Elongation (%)	10	9	14	13	13
K_{IC} (ksi$\sqrt{in}$)	48	55	115	LS 104, SL 95	109
K_{ISCC} (ksi$\sqrt{in}$)**	13	16	23	LS 85, SL 88	27
**** in 3.5% NaCl**					

THIS PAGE INTENTIONALLY LEFT BLANK

DISTRIBUTION:

NAVAIRSYSCOM (AIR-4.0T - Dr. James Sheehy), Bldg. 2109, Room N122 (1)
48150 Shaw Road, Patuxent River, MD 20670
NAVAIRSYSCOM (AIR-4.3), Bldg. 2187, Suite 3340 (1)
48110 Shaw Road, Patuxent River, MD 20670-1906
NAVAIRSYSCOM (AIR-4.3T – Jerry Rubinsky), Bldg. 2187, Suite 3322 (1)
48110 Shaw Road, Patuxent River, MD 20670-1906
NAVAIRSYSCOM (AIR-4.3.4 – Darrel Tenney), Bldg. 2188 (1)
48066 Shaw Road, Patuxent River, MD 20670-1908
NAVAIRSYSCOM (AIR–4.3.4.1 – Robert Kowalik), Bldg. 2188 (1)
48066 Shaw Road, Patuxent River, MD 20670-1908
NAVAIRSYSCOM (AIR–4.3.4.1 – Eun U. Lee), Bldg. 2188 (25)
48066 Shaw Road, Patuxent River, MD 20670-1908
FRC/ISSC Jacksonville (AIR-4.3.4) (1)
Naval Air Station, Jacksonville, FL 32212
FRC/ISSC Jacksonville (AIR–4.3.4.6 – John Benfer) (1)
Naval Air Station, Jacksonville, FL 32212
Office of Naval Research (Code 35 – William Nickerson) (1)
875 N. Randolph St., Room 1143B, Arlington, VA 22203
NAVAIRSYSCOM (AIR-4.0), Bldg. 407, Room 116 (1)
22269 Cedar Point Road, Patuxent River, MD 20670-1120
DTIC (1)
8725 John J. Kingman Road, Suite 0944, Ft. Belvoir, VA 22060-6218